Proceedings of the 8th World Congress on Momentum, Heat and Mass Transfer (MHMT'23)
Lisbon, Portugal – March 26 – 28, 2023
Paper No. ICMFHT 127
DOI: 10.11159/icmfht23.127

Design and Analysis of a Cryogenic Unsteady Flow Experiment through a Propellant Assisted Valve

Jorge Pinho[1], Arnaud Magette[2], Maria Teresa Scelzo[1], Jean-Baptiste Gouriet[1], Johan Steelant[3]
[1]von Karman Institute for Fluid Dynamics,
Chaussée de Waterloo 72, 1640 Rhode Sint-Genèse, Belgium
Jorge.pinho@vki.ac.be
[2]Safran Aero Boosters
Rte de Liers 121, 4041 Herstal, Belgium
[3]ESTEC - European Space Agency
Keplerlaan 1, 2201 AZ Noordwijk, The Netherlands

Abstract - This paper provides a technical assessment of the design definition and justification of an experimental activity to be conducted on unsteady cryogenic flows through valves and orifices with nitrogen. The primary application of this study serves engine propellant assisted valves used in space launchers, but it is expected that results can also be extended and valorised to other sectors dealing with cryogenic flows. This research aims at understanding the challenging flow physics occurring in cryogenic valves dealing with both liquid and vapour fluid state including phase change, during their opening and closure operation, providing a reliable and complete experimental database that can be used for validation of unsteady two-phase flow numerical models. For this objective, the complex valve design is simplified, and several orifice sizes and geometries are proposed individually and simultaneously to characterize the unsteady cryogenic flow. Furthermore, initial temperature conditioning of the experimental setup ranging from cryogenic to ambient values will allow covering different flow regimes. In the first part of the paper, the background research and motivations are introduced. Secondly, the design of the experimental setup and expected operating conditions are described including the analysis of the proposed instrumentation: mass flow rate, pressure, temperature, and flow visualization. Each measurement technique is described and analysed. In the third part, a thermal-mechanical FEM study is presented to provide estimations of maximum deformations and mechanical stresses expected in the different test section materials during the experimental tests, therefore supporting the selection of the test section materials and manufacturing processes. Fourthly, a simplified 1D unsteady flow modelling tool that couples mass, momentum and energy equations is proposed to evaluate the flow characteristics for the future experiments. Preliminary results of the 1D model are presented to support this design of experiment.

Keywords**:** cryogenic valve design, filling cavity, orifice, two-phase flow, propellant assisted valve, cavitation

1. Introduction

Propellant assisted valves (PAV) include an actuator assisted by a hydro-pneumatic muscle to move the main poppet. The actuator is used to manage the pressure inside an intermediate chamber by opening or closing inlet and outlet apertures (pilot stage). The pressure inside this intermediate chamber generates a force on a piston that causes the displacement of the main poppet. Thus, the actuator itself must overcome the upstream pressure on a limited area (much smaller than the main tightness area) which allows reducing the required power and finally its mass. In the case of an assisted valve, the actuator is coupled with a pilot poppet allowing its displacement with only a limited pressure available. Fig. 1 illustrates the opening and closing steps of a PAV with an upstream cavity, i.e., the intermediate chamber which is pressurized when the valve is closed and emptied when the valve is opened.

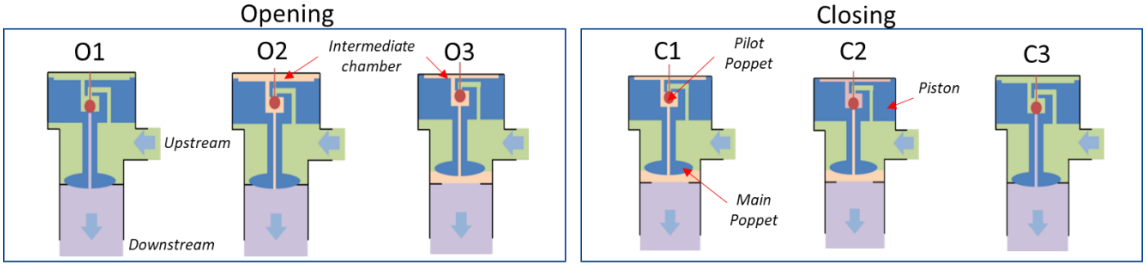

Fig. 1: Opening and closing steps of a typical PAV with an upstream cavity (intermediate chamber).

In step O1 on the left, the valve is closed. The intermediate chamber is full of fluid at upstream pressure. The pressure force balance acting on the poppet and piston assembly is acting toward closing. In step O2, the actuator is powered for opening. The pilot poppet moves up which results in opening the draining channel and in closing the filling channels. The intermediate cavity is now connected to the downstream of the valve, allowing its emptying. Finally, in step O3, the pressure inside the intermediate cavity is sufficiently low so that the pressure force balance is now towards opening. The poppet and piston move up and the valve is open. After opening, the cavity pressure may continue decreasing, which results in increasing the holding open force. Similarly, the closing process from C1 to C3 is the opposite as the one given for opening case.

During the operation of a PAV, the fluid state might result in liquid or gas depending on both pressure and temperature conditions. Moreover, important thermal considerations are required for the operation of such valve in cryogenic environment as it is the case for propellant valves used in space launchers. These pressure and temperature ranges influence considerably the opening and closure valve response time although the physical root cause is not entirely identified. From one side, it is known that mass flux through an orifice tends to be reduced in presence of two-phase and choked flow conditions. On the other hand, the heat transfer mechanism of a filling cavity depends on several parameters such as the initial wall temperature, fluid filling rate, pressure, and temperature conditions. The combination of these factors may result in significant changes of the opening and closing valve response time. The present research aims at experimentally reproducing these phenomena in simplified orifice geometries to allow building a reliable and complete experimental database that can be used for validation of numerical models.

2. Design of experiment

2.1. Experimental Setup

The test bench CHIEF, constructed during past ESA-GSTP activity "Experimental Investigation of Cryogenic Two-Phase Flow", L. Peveroni [1] and illustrated in Fig.2, has been selected to host the new test section. The cryogenic fluid (liquid nitrogen, LN2) is stored in a pressurised ranger with a capacity of 176 litres. The ranger is connected to a pressurization unit composed of gas nitrogen (GN2) bottles and pressure regulators to supply LN2 at an adjustable and stable pressure (up to 8 bars abs). The reservoir is placed outside the laboratory but sufficiently close to the test facility to limit as much as possible long transfer lines.

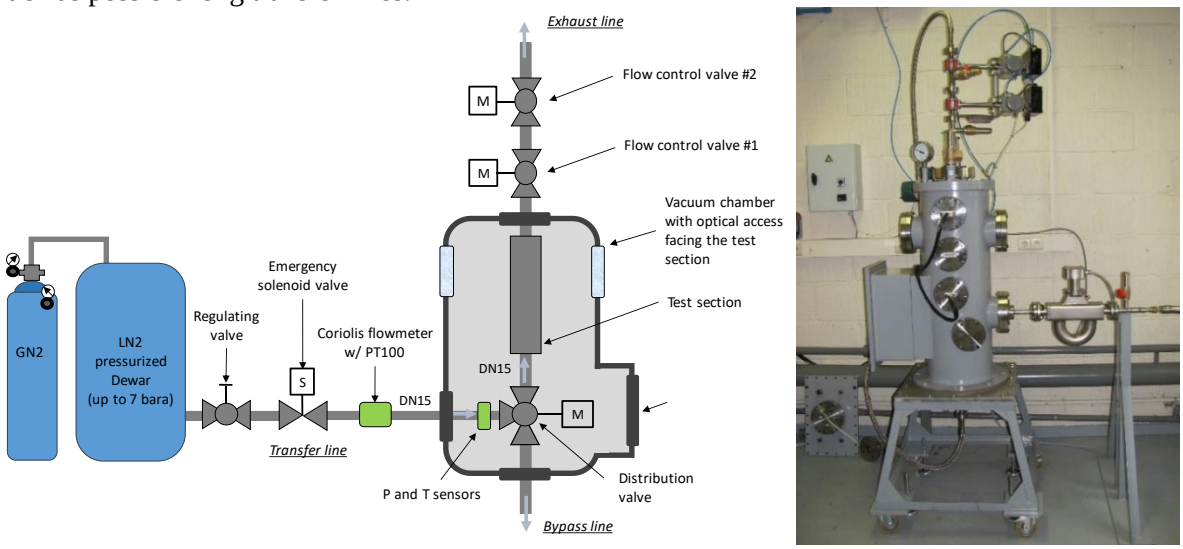

Fig. 2: CHIEF facility in its original configuration.

The bypass line used to insure full-liquid condition at the inlet of the test section is connected to the other lines by mean of a 3-way valve coupled to an electro-pneumatic actuator and solenoid valve for remote control. The instrumented

test section is mounted vertically and connected to the test bench through DN15 flanges. A cryogenic ball valve mounted downstream the test section allows to modulate and control the backpressure. Both the bypass and exhaust lines are connected connected to an evaporating tank installed outside the laboratory from which the vapour is released to the atmosphere through through a chimney. Finally, a vacuum chamber equipped with several electrical and pipe feedthroughs as well as with view view ports for flow visualisation surrenders the test section to ensure its thermal insulation from the external environment. environment.

2.2. Test Section

The new proposed test section is detailed in Fig. 3 and allows the testing of two distinct configurations. In the first configuration mode, shown on the left side, a single orifice is to be characterized. Measurements include mass flow rate, pressure, and temperature upstream and downstream the orifice. The orifice discharge coefficient at steady regime will be determined with LN2 and GN2 fluid conditions. A total of 3 orifices have been sized for this experiment to be representative of the sections and geometries in a real PAV: 2 circular orifices with ø 2.5mm and ø 0.8mm, and a rectangular orifice with a section of 0.5x3.0mm^2. In the second configuration mode shown on the right side of Fig. 3, two different sized orifices are mounted in the test section separated by a cavity volume of 38mL. The combination of different orifice sizes positioned at upstream and downstream locations will allow to investigate the cavity pressurization and depressurization modes.

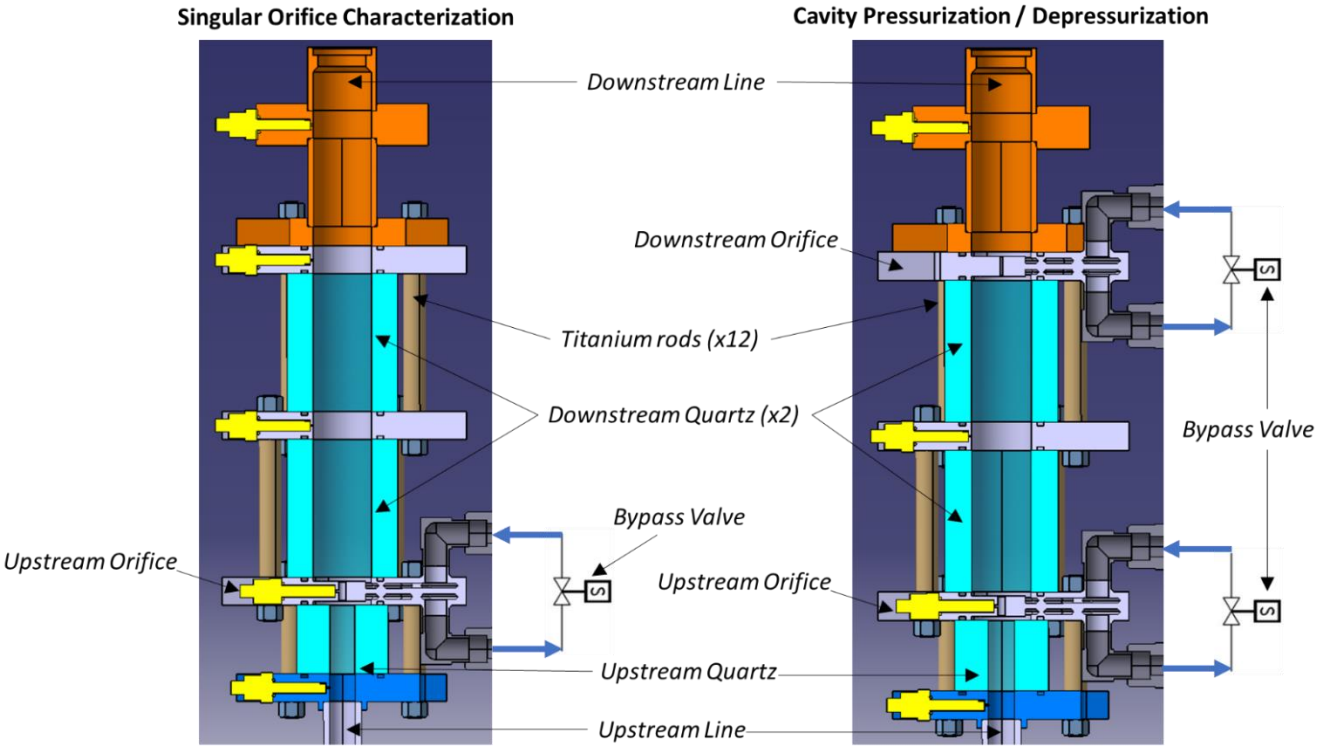

Fig. 3: Test section of the experiment: single orifice (left) and cavity pressurization / depressurization (right).

The orifice plates have been designed based on previous work of J.B. Gouriet [2] to include an additional bypass section allowing enough flow rate to cool down the entire test section during the chilldown phase prior to the experiment. This bypass flow is controlled by means of a solenoid cryogenic valve (model KB15 from COAX) mounted between the upstream and downstream side of each orifice plate to be manufactured by 3D metal additive technology. The 3D printing of the orifice plate allows the definition of internal channels and prevents the need of welding operations, significantly reducing the time required for assembling the components. The test section will host a total of three quartz modules: 2 larger modules with inner diameter ø21 mm will be placed downstream the first orifice while another smaller module (inner diameter ø9.2mm) will be placed upstream. The external surfaces are planar (finished with flame polishing) to optimize the flow visualization

quality. Each quartz module will be placed between two flanges allowing a clearance of 0.1mm, meaning that at room temperature the quartz modules will not be compressed by the flanges (except some negligeable effort resulting from compression of the axial seals). This clearance is guaranteed by the usage of titanium grade 5 rods ø8 mm which are to each flange. Each quartz module assembles 4 rods; hence three modules require a total of 12 titanium rods. The location of the titanium rods (and consequently the position of the flange holes) has been defined to allow full optical to the test section.

2.2. Temperature and Pressure measurements

Temperature measurements are performed with cryogenic silicon diodes Lakeshore DT-670B-SD to measure the wall temperature close to the installation port of the pressure sensors thermal correction. The response time of the silicon diode sensors can be significantly affected by the assembly design. Lakeshore diodes have a response time of the order of 100 ms at 77 K and 200 ms at 305 K (according to manufacturer's technical sheet [3]). However, in case of a poor contact between the sensor diode and the solid wall, an additional thermal resistance can affect the rapidity of the sensor response. Typically, these sensors are glued by means of a dedicated cryogenic grease with a very high thermal conductivity that ensures a non-permanent thermal anchoring of the diode inside the port cavity. Nevertheless, this additional layer of grease increases locally the thermal resistance. Different scenarios have been investigated by means of a simplified thermal analysis described on the left of Fig. 4. The stainless steel thermal conductivity has been derived from D. Mann [4] (k_{SS}=10W/m.k), while properties for cryogenic grease were obtained from manufacturer datasheet Apiezon [5] (k_G=0.194W/m.k). Relations presented on the left side of Fig. 4 allow to estimate the response time of the sensor with additional grease thermal resistance (it is assumed that without cryogenic grease, the sensor has a response time of 100ms). By reducing the size of the rectangular port pockets to 1.2 x 2.2 mm^2 and manufacturing tolerances +0.1/0 mm, the response time of the diodes sensors is estimated to be in the range 100ms - 310ms, which is crucial for the present experimental campaign (specially for the cavity pressurization/depressurization tests shown in Fig. 3).

For the pressure measurements, cryogenic miniature ruggedized pressure transducers from Kulite Semiconductor (CTL-190M series) have been selected for both steady and unsteady regimes and are distributed at several axial points of the test section. The transducers installation ports have been designed in such way that sensors are recessed with respect to the pipe internal wall to protect the sensor from impurities of the line and avoid any flow perturbation inside the channel as given on the right side of Fig. 4.

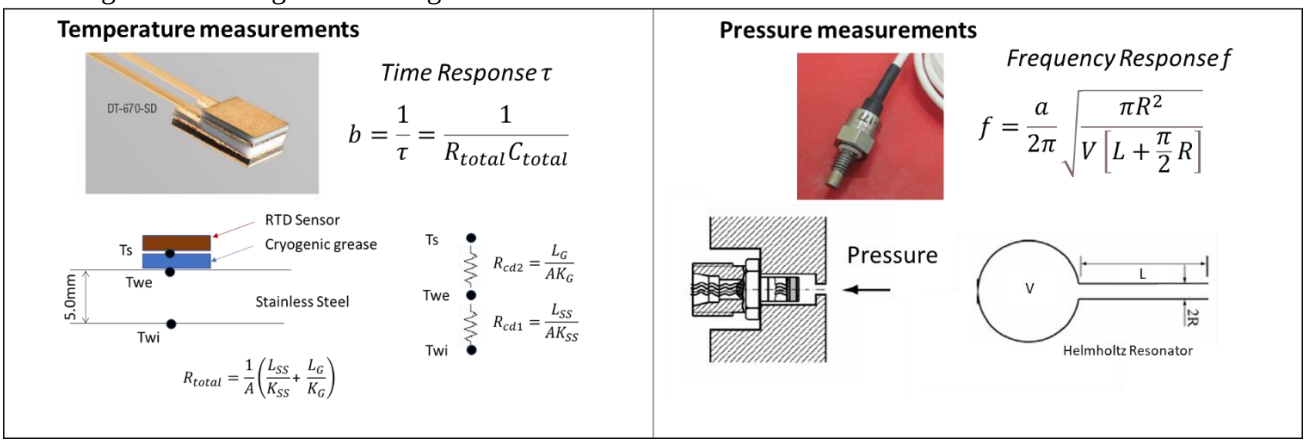

Fig. 4: Analysis to estimate temperature and pressure sensor response time.

This second point is more critical for the pressure measurements to be performed in the bypass-orifice modules as channels are normally smaller than the pressure sensor itself (sensor has ø3.8 mm while circular orifice is ø2.5 mm and rectangular orifice 0.5x3.0 mm^2). Therefore, to maintain similar performance among the different sensors, it was decided to keep the same recessed design in all port's location. The frequency response of the transducer and data acquisition system must be considered. In particular, the recessed design reduces the frequency response with respect to

the flush mounted case. Based on previous work of D. Wulff [6], the recessed sensor frequency response *f* is estimated by the Helmholtz Resonator relation shown on the right side of Fig. 4. Results are summarized in Table 1 including the propagation associated to the uncertainty of each variable.

Table 1: Uncertainty propagation of manufacturing tolerances in the pressure sensor frequency response.

	Nominal	Tolerances
Fluid speed of sound *a [m/s]*	719	N/A
Radius of the pipe *R [mm]*	0.4	0.375-0.425
Length of the pipe *L [mm]*	1.3	1.075-1.525
Volume cavity *V [mm^3]*	2.77	2.77-5.54
Frequency response [kHz]	*35.1*	*22.2-39.2*

The minimum frequency response will be of the order of 22.2kHz which is still sufficient to resolve the flow unsteadiness linked to liquid vaporization in the orifice (dominant frequencies <4kHz were measured during a previous campaign, see work of C. Esposito [7]).

3. FEM thermal-mechanical analysis

This section presents a FEM thermal mechanical analysis performed during the sizing and design of the present experiment allowing to estimate the temperature field of the hardware as well the maximum deformations and mechanical stresses expected during the experimental tests. The analysis has been performed with ANSYS 2021 R2 integrating both thermal steady state and structural modules. A standard adaptive sizing mesh is generated in the model with 4 levels of refinement. A smooth transition inflation is enabled in regions requiring higher level of meshing. All remaining parameters are controlled automatically by the software. The total number of nodes and elements are 166,884 and 65,988, respectively. All contact surfaces between different parts are assumed to be bonded connections, without any thermal resistance. In terms of thermal boundary conditions, an external heat transfer convection towards the vacuum chamber has been considered (hext=2W/m^2.K at 295K) based on Nusselt number correlation $Nu = 0.59{Ra_L}^{1/4}$ applied to a vertical plate [8]. For the calculation of Rayleigh number Ra_L, air properties were evaluated at reduced pressure 20mbar and film temperature conditions $\frac{T_{pipe}+T_{amb}}{2} = \frac{90+280}{2} = 185K$. On the other hand, for the internal surfaces in contact with the cryogenic fluid, a significant higher forced convection has been imposed (hint=1000W/m^2.K at 90 K) to guarantee a constant temperature in all internal surfaces and reduce the computational time. Please note this last boundary condition is not physical, typical values would range from 100-300W/m^2.K; nevertheless it is a more conservative scenario since it forces the internal temperature to be around 90K. Regarding structural boundary conditions, it is assumed that the upstream surface flange is fixed while the downstream surface flange supports the remain weight of the test setup. A total mass of 10kg (~100N) has been estimated for the downstream line which is connected to the test section. Finally, a pressure boundary condition is applied on the upstream surface of the upstream orifice. This scenario simulates the case in which liquid nitrogen is flowing in the test section with a maximum pressure of 100bar. Mechanical properties were derived from different cryogenic databases available for Stainless steel 316, Titanium Grade 5/Ti-6AI-4V and Quartz Glass materials: thermal conductivity, specific heat, Young Modulus, density, Poisson ratio [4] [9] [10] [12], and thermal expansion coefficient [11]. Yield Strength properties have been based on manufacturer datasheet at ambient temperature (3D printing material Stainless Steel 316L [13]), although a factor of $\sigma_{100K}/\sigma_{300K} = 1.4$ is reported for the ratio between cryogenic and ambient temperatures [12].

Results of the FEM thermal-mechanical analyses are summarized in Fig. 5. The test section overall temperature field is given in c) with identification of the maximum temperature region (~113K) in the mid-span of the titanium rods supporting the assembly. These results are expected since the rod mid-span elements are located the most far away from the wet surface which naturally is the coldest point at 90K. The regions located nearby the orifice flange show significant lower thermal gradient because of their improved cooling effect. Both scenarios are detailed in a) and b) that presents the temperature

contours sections of both intermediate and orifice flanges (both scales were adjusted for visualization purposes). The intermediate flange is less efficient than the orifice flange because of its much smaller heat transfer area. The maximum temperature gradient is of the order of ~10K for the intermediate flanges and ~3.7K for the orifice modules between wet and external surfaces.

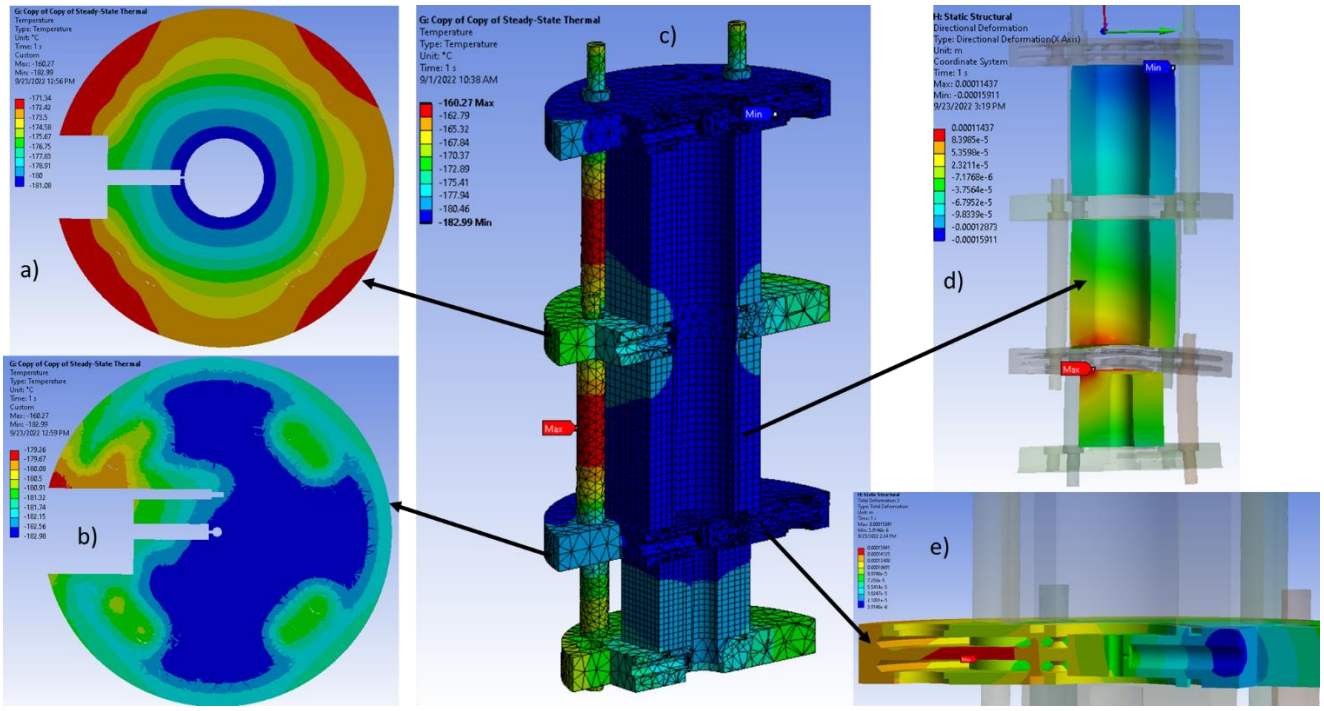

Fig. 5: FEM thermal-mechanical analysis results. Thermal field of a) intermediate flange without bypass cooling; b) upstream orifice flange with bypass cooling and c) test section. Maximum displacements of d) quartz modules and e) upstream orifice flange.

An important result from the analysis is the understanding of the components behaviour during the experimental tests at cryogenic temperatures. The quartz modules having the lowest yield strength among the different components (48MPa), were sized to prevent any mechanical compression resulting from adjacent parts (either flanges or bypass modules manufactured in stainless steel). This is guaranteed by a tolerance (+0.1mm) defined for the titanium rods length before the assembly of the components. On the other hand, it is important to verify the maximum deformations obtained for the quartz modules in case a perfect contact with the flanges would occur. This scenario is illustrated in d) in which the directional deformation is shown for the different quartz modules, with identification of maximum and minimum deformations of +/-0.1mm. Finally, maximum displacements of 0.16mm are estimated in e) (internal surface of the orifice flange) resulting in Von-Mises stresses of 289MPa. A final safety factor of 1.9 is established for the 3D printing parts in stainless steel 316L.

4. Flow modelling

A simplified 1D unsteady flow modelling tool that couples mass, momentum and energy equations is proposed in Fig. 6 to evaluate the flow characteristics for the future experiments. The model consists of 13 lumped nodes ψ distributed along the axial direction of the test section, containing variables of pressure and enthalpy. The pressure at the outlet is fixed at 1bar, while the inlet pressure is set at 8.4bar according to previous experiments [7]. Mass flow rate is calculated between each node with appropriate discharge coefficients. The mass flow rate between (ψ_2 - ψ_3) and (ψ_6 - ψ_7) is the sum of the mass flow through bypass and orifice sections. Differential equations of pressure and enthalpy are computed at each node with a standard ODE solver. Finally, liquid nitrogen properties such as density and enthalpy are evaluated from NIST database [14] at isothermal conditions (90K).

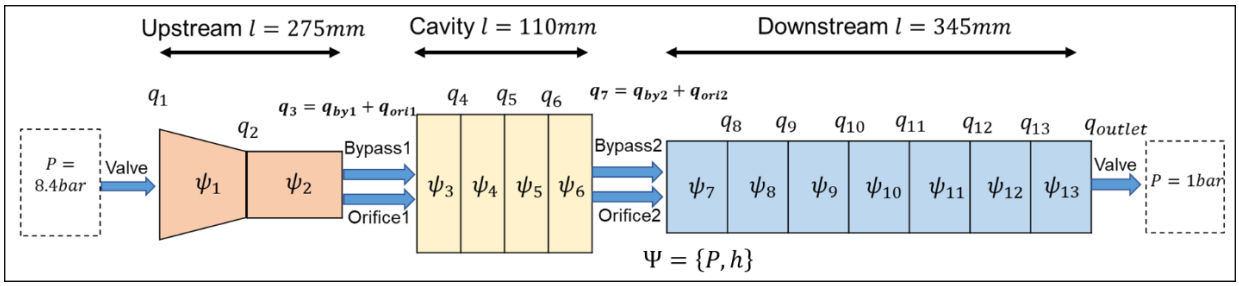

Fig. 6: Schematic of 1D unsteady model.

The model is limited for the case of liquid single-phase flow and serves this work simply to support the design and mimic the expected experiments. A first validation is presented on the left side of Fig. 7 against available data from [7] in which a singular orifice ø2.5 has been tested. This experiment reproduces a single orifice characterization in which the bypass valve starts closing at t=23s and takes 170ms to complete its closure. The downstream pressure difference between experimental and numerical data is lower than 0.5 bar, corresponding to 10% of the nominal pressure. On the right of Fig. 7, the same model is then tested for the cavity pressurization mode (as earlier described on the right side of Fig. 3), to reproduce the pressure history expected in the future experiments. The upstream orifice has ø2.5 while the downstream orifice is smaller ø0.8. The closing time of each bypass solenoid valve is kept to 170ms although a delay of 2s is defined between the closure of the upstream and downstream bypasses, at t=23s and t=25s, respectively.

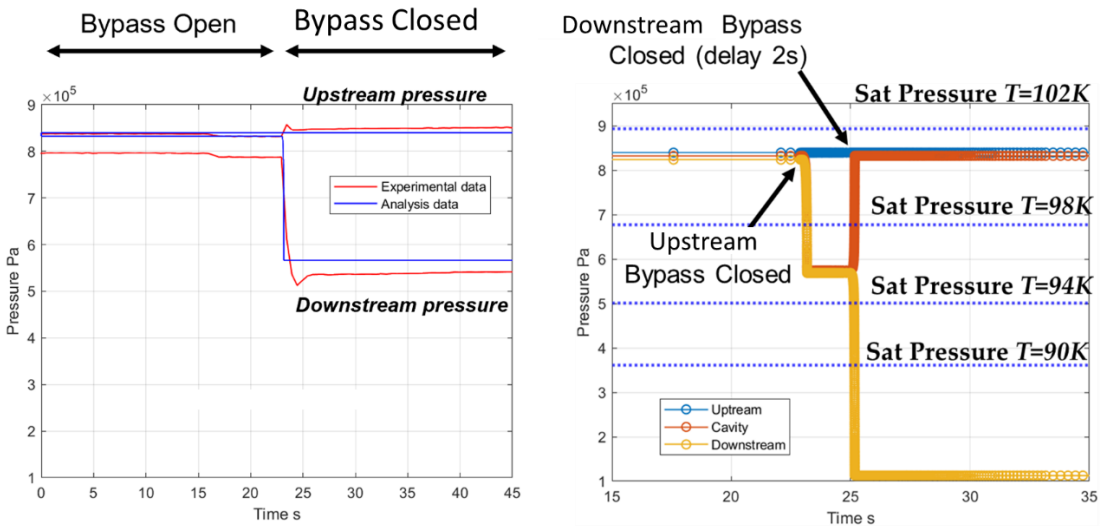

Fig. 7: Pressure profiles of unsteady analysis. Left side: single orifice ø2.5 during opening of single bypass. Right side: Cavity pressurization mode with upstream orifice ø2.5 and downstream orifice ø0.8.

At t=0 both bypass valves are fully open, so pressure is uniform along the test section. When upstream bypass valve is closed at t=23s, the cavity pressure decreases and stabilizes at about 5.7bar. The next step is the closure of the downstream bypass valve at t=25s which results in the cavity pressurization since inlet flow rate is higher than outlet flow rate. In the same figure, saturation pressure thresholds have been defined at different initial temperatures ranging from 90K to 102K. Following scenarios are given: i) if the initial cavity temperature is above 102K, the flow will always be gas during the entire test (all curves are below the saturation pressure at 102K); ii) if the cavity initial temperature is around 98K, the first depressurization will generate a two-phase flow which will condense after the closure of the downstream bypass and consequent cavity pressurization; iii) When the initial cavity temperature is lower than 94K, all experiment is performed in liquid condition (this case has been the one assumed for all the analysis presented so far).

5. Conclusions

The design definition and justification of the test setup for the acquisition of a steady and transient database on two-phase flow (liquid nitrogen) through a cavity has been described and discussed in this paper. These experiments generating a novel and well-documented database of the cryogenic two-phase flow through a filling or emptying cavity, which can provide important design guidelines for future propellant assisted valves. Main hardware components and measurement techniques of the proposed experiments were presented and analysed. Design calculations demonstrate that both temperature and pressure sensors have an adequate response time to capture the fluid physics.

A dedicated FEM thermal-mechanical analysis was performed to justify and validate the adopted design and support the test section materials selection: stainless steel 316L, Titanium Grade 5 and Quartz Glass. 3D additive metal printing has been selected for the manufacturing of the orifice flanges in stainless steel 316L, as FEM analysis results in a safety factor of 1.9 assuming maximum test conditions of 100bar. Finally, a simplified 1D model has been included to mimic the experimental tests and enhance the pressurization / depressurization regimes to be implemented in the tested cavities. Although numerical results are useful for the experiments preparation, the model is very simplistic as does not consider heat transfer from surroundings to the test section neither inertia effects that can arise during pressurization / depressurization of the cavity. These phenomena are very complex and will require dedicate experimental data to be properly addressed numerically.

Acknowledgements

The authors acknowledge S. Borrey for the test section CAD design, and Y. Takeda for the implementation of the 1D numerical model. This study is supported by the ESA through the General Support Technology Programme activity Experimental characterization and modelling of transient multi-phase operated propellant-assisted shut-off valve, ESA Contract n°4000137720/22/NL/MG/rk.

References

[1] L. Peveroni, “TN 3100C: Design of the test facility” in GSTP Experimental investigation of Cryogenic Two-Phase Flow, 2015.
[2] J.B. Gouriet, “TN4200: Technical description of the manufactured breadboard model and facility adaptation” in GSTP 6 – Experimental characterization of transient flow phenomena in cryogenic fluids, 2018.
[3] Lakeshore Cryotronics, “Temperature Measurement and Control Catalogue”, in Appendix G: Sensor Temperature Response, 2022.
[4] D. Mann, “LNG Materials and Fluids”, National Bureau of Standards, Cryogenics Division First Edition, 1977.
[5] Apiezon. “SCB Datasheet Apiezon L,M+N”, 2022.
[6] D. Wulff, “Unsteady Pressure and Velocity Measurements in Pumps”, in Design and Analysis of High-Speed Pumps (pp. 4-1 – 4-34). Educational Notes RTO-EN-AVT-143, Paper 4, 2006
[7] C. Esposito, “Study of Cryogenic Transient Flows. The impact of the fluid thermosensitivity on cavitation”, PhD Thesis KULeuven and von Karman Institute for Fluid Dynamics, 2020.
[8] D. Incropera, “Fundamentals of Heat and Mass Transfer”, 6th Edition, John Willey & Sons, 2006.
[9] W.T. Ziegler, “Specific Heat and Thermal Conductivity of Four Commercial Titanium Alloys From 20 to 300K”, in Advances in Cryogenic Engineering Vol. 8, 1963, p. 268-277, 1963.
[10] Simon, “Cryogenic Properties of Inorganic Insulation Materials for ITER magnets: a review.”, in NISTIR 5030, National Institute of Standards and Technology, 1994.
[11] C, Gniewek, “Thermal Expansion of Technical Solids at Low Temperatures”, National Bureau of Standards, Monograph 29, 1961.
[12] Schwartzberg, “Cryogenic Materials Data Handbook”, Air Force Materials Laboratory TDR-64-280 Volume I, 1970.
[13] SLM, “Material Data Sheet 316L/1.4404/A276”, 2017.
[14] NIST, “Thermophysical Properties of Fluid Systems”, 2011.